Ann. Rev. Nucl. Part. Sci. 1987. 37: 1–31

COMPUTER SIMULATIONS OF NUCLEAR DYNAMICS

David H. Boal

Department of Physics, Simon Fraser University, Burnaby, British Columbia V5A 1S6, Canada

CONTENTS

1. INTRODUCTION

The problem of describing a nuclear reaction is obviously a very complicated one that does not lend itself easily to analytical treatment. There are not a very large number of particles in the system, yet the system is not always so dilute that the interactions are strictly two-body in nature. The energy and distance scales are such that quantum mechanical effects are certain to be critically important to some stages of the reaction. While statistics may dominate certain experimental observables, on average the systems begin the reaction with a phase space configuration very different

0163–8998/87/1201–0001$02.00

from that of the reaction products, and only part of the system may reach any form of equilibrium.

About a quarter of a century ago (107) it was recognized that computers could be used to simulate some aspects of nuclear reactions. Even though the machines were of limited speed and memory judged by today's standards, the experimental observables that were the subject of the simulations were also relatively simple. As the experimental measurements have become both more detailed and more accurate, so too has the need for more sophisticated simulations.

As an illustration of the physics ingredients necessary for a successful simulation of the time evolution of a nuclear reaction, we show in Figure 1 a simulation (14) of a Ca+Ca collision at a bombarding energy of 200 MeV/nucleon in the lab frame. The figure shows the positions of the nucleons in a central (zero-impact parameter) collision shortly after the period of maximum overlap of the projectile and target. One can see that there are significant density fluctuations present, rendering a simple description of the process in terms of homogeneous nuclear matter inappropriate. Similarly, the nuclear material has not totally vaporized to produce a dilute gas, and hence quantum effects such as the Pauli exclusion principle remain important. Several regions of high density will emerge at the end of the reaction as fragments.

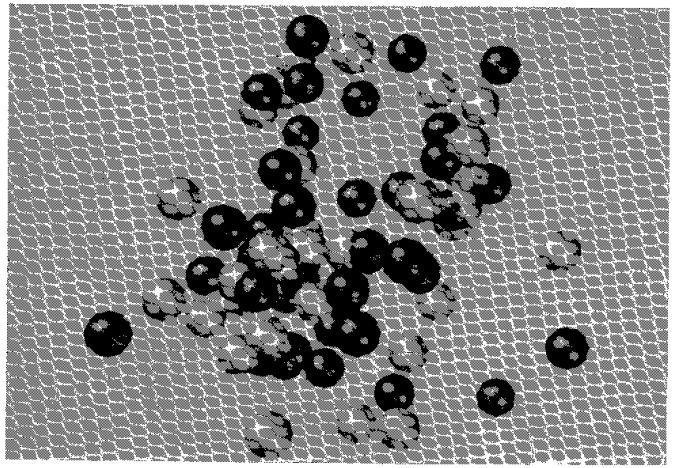

Figure 1 Simulation of a central collision of two calcium nuclei. The time evolution was stopped shortly after the time of maximum overlap (14).

Figure 1 provides an example of how complicated the reaction process can be; nevertheless, there *are* processes that lend themselves to treatment analytically. Simple knockout or transfer reactions are unlikely to need the computational effort required to describe a nearly central heavy ion collision. Further, some characteristics of the reaction products may find their description in statistical mechanics because of ensemble averaging or other causes.

The purpose of a computer simulation is not simply to describe reactions; it allows us to test the sensitivity of the reaction to the nuclear physics incorporated in the simulation. Thermal model analyses (27, 54, 82a) of intermediate energy nuclear reactions indicate that the reaction trajectories traverse regions characterized by temperatures ranging from a few to many tens of MeV. In this temperature range, infinite nuclear matter shows several interesting properties. The pressure vs density diagram predicted (26) for a gas of neutral nucleons interacting via a zero-range Skyrme potential is shown in Figure 2. The isotherms are labeled by their respective temperatures (measured in MeV). For densities much above normal nuclear matter density, the pressure rises fairly rapidly. This region may be accessible in the early stages of a high energy, heavy ion reaction (125).

The form of the isotherms is reminiscent of that of a van der Waals fluid: the usual Maxwell construction yields a phase diagram with distinct liquid and vapor phases and with a critical temperature of 15.3 MeV for the parametrization used in the figure. Of particular interest is the mechanical instability region (21) $dP/d\rho < 0$, in which density fluctuations grow with time. As mentioned in the discussion of Figure 1, similar density fluctuations may be important for understanding the emission of complex fragments. One of the challenges for simulations is to make the connection between experimental measurements and the physics, such as the equation of state, that underlies the reaction mechanism.

Because the field of computer simulations is advancing so rapidly, several of today's burning issues will be resolved and replaced by new ones between the writing of this review and its publication. While reference is made to current controversial questions, they do not form the bulk of the material in this review. Rather, we examine several different approaches to numerical simulations and highlight the similarities and differences between them. Results from several techniques are illustrated and contrasted. In choosing examples for the application of the techniques, emphasis is placed on examining general issues in reaction dynamics and the properties of nuclear matter, rather than dealing with specific experimental comparisons.

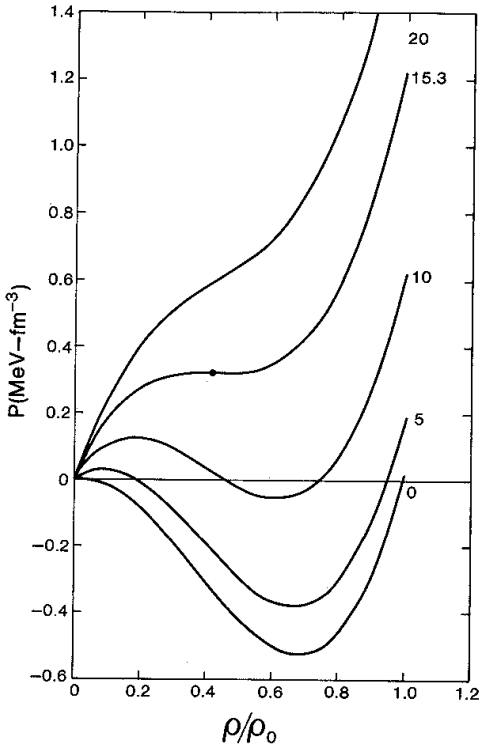

Figure 2 Equation of state predicted for neutral nuclear matter using a zero-range Skyrme-type interaction. The temperatures of the isotherms are given in MeV (26).

2. HIGHLY EXCITED NUCLEAR MATTER

2.1 *The Nuclear Equation of State*

The nucleon-nucleon interaction is repulsive at short distances and attractive at large distances. This behavior is qualitatively similar to the molecular interaction of substances that exist in liquid and gaseous phases. Based on such considerations, nuclear matter also may be expected to exist in liquid and gaseous phases (52, 53, 100, 103, 118, 120).

The properties of nuclear matter at high densities have been investigated for some time because of their importance in astrophysics, for example, in

the study of the formation and characteristics of neutron stars (see 100 and references therein). The problem of accessing the equation of state experimentally has only been addressed in more recent years. Research has focussed on two main areas: the determination of the nuclear equation of state at high densities and the search for evidence of a liquid-vapor phase transition.

To extract the essential features of the equation of state, we will adopt a simple model (26, 67, 104) in which the nucleon-nucleon potential is approximated by a zero-range Skyrme-type interaction:

$$V_{12} = \left[-t_0 + \frac{t_3}{6}\rho\right]\delta(\mathbf{r}_1 - \mathbf{r}_2), \qquad 1.$$

where ρ denotes the density at $(\mathbf{r}_1+\mathbf{r}_2)/2$ for nucleons at positions $\mathbf{r}_1$ and $\mathbf{r}_2$. The parameters t_0 and t_3 in Equation 1 are chosen to fit the properties of cold nuclear matter. The potential energy associated with this interaction has the form

$$U(\rho) = -\frac{3}{4}t_0\rho + \frac{3}{16}t_3\rho^2. \qquad 2.$$

This is commonly referred to as a "stiff" equation of state. There are many other popular parametrizations of the equation of state that also use a power law form (for a more detailed discussion, see 45, 109, 110, 125, 126):

$$U(\rho) = -a\rho + b\rho^{\sigma}. \qquad 3.$$

The choice of $\sigma = 7/6$ is referred to as a soft equation of state. The pressure corresponding to Equation 2 can be expressed as the sum of two terms: a kinetic term,

$$P_{\text{kin}} = -\frac{T}{V}\ln z, \qquad 4.$$

where z is the grand partition function for independent fermions, and an interaction term,

$$P_{\text{int}} = -\frac{3}{8}t_0\rho + \frac{1}{8}t_3\rho^2. \qquad 5.$$

A particular choice of t_0 and t_3 yields (26) the pressure vs density curves shown in Figure 2. The phase diagram associated with Figure 2 is shown

in Figure 3. Maxwell's construction is used to find the liquid-gas coexistence curve (LGC); the isothermal (ITS) and isentropic (IES) spinodal curves are defined by the conditions $(\partial P/\partial \rho)_{T=0}$ and $(\partial P/\partial \rho)_{S=0}$, respectively. Also shown in the figure are dotted curves of constant entropy (S/A). A more detailed discussion of the properties of the phase diagram can be found in (67).

The boundaries of the phase diagram are not particularly sensitive to the specific choice of parametrization for the nucleon-nucleon interaction; rather similar results were obtained by two groups (26, 104) using different parametrizations. However, the inclusion of the Coulomb interaction and the finite size of the nucleus lower the predicted value of the critical temperature considerably (32, 83, 131).

The trajectory that a reaction will take through the phase diagram varies according to projectile and energy. As discussed below, proton-induced reactions are unlikely to compress the nucleus very much, and the reaction trajectory of the target region is likely to involve excursions through the coexistence region and perhaps into the mechanical instability region (26).

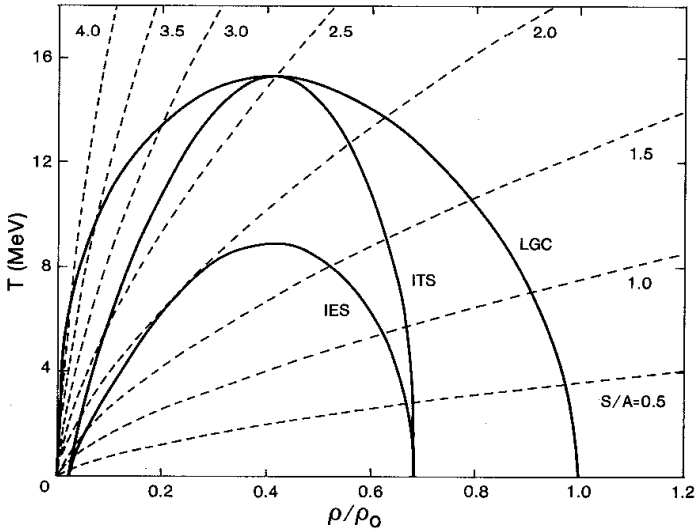

Figure 3 Phase diagram of neutral nuclear matter. Isentropes of given values of S/A are shown by the dashed curves. The liquid-gas coexistence curve is labeled as LGC; the isothermal and isentropic spinodals are labeled as ITS and IES, respectively (26).

Central collisions of heavy ions, on the other hand, produce considerable compression and heating. Such systems, once thermalized, should expand approximately isentropically (19), perhaps passing near the critical point (81).

2.2 *Hydrodynamics*

The reaction trajectory can be determined by solving the equations governing the time evolution of quantities such as the energy density, number density, etc. An example (133) of an early attempt to do this analytically is the use of the diffusion equation to follow the dissipation of heat deposited in nuclear matter. However, the complex geometry of a reaction generally requires that the equations be solved numerically.

If the mean free path of a nucleon in nuclear matter is sufficiently short, then a local equilibrium may be established within the reaction zone and the region may evolve according to hydrodynamics. Estimates of the mean free path (86) suggest that it is of the order of the internucleon spacing. Although this does not put one well into the hydrodynamic regime, neither is it so far away from that regime that hydrodynamics is irrelevant. The attraction of hydrodynamics is, of course, the simplicity of its ingredients: conservation laws and an equation of state. The sensitivity of experimental observables to the equation of state can then be found in a straightforward manner.

In relativistic form, the ideal single-fluid hydrodynamic equations read (45, 102, 110, 126):

$$\frac{\partial N}{\partial t} + \nabla \cdot (\mathbf{v}N) = 0, \qquad 6.$$

$$\frac{\partial \mathbf{M}}{\partial t} + \nabla \cdot (\mathbf{v}\mathbf{M}) = -\nabla p, \qquad 7.$$

$$\frac{\partial E}{\partial t} + \nabla \cdot (\mathbf{v}E) = -\nabla \cdot (\mathbf{v}p), \qquad 8.$$

where N, $\mathbf{M}$, and E are the nucleon number density, momentum density, and energy (including rest mass energy) density, respectively, in the laboratory (or computational) frame of reference. The velocity $\mathbf{v}$ of the fluid frame can be defined in more than one way. The common choice in nuclear problems is to demand that the baryon number flux vanish in the fluid frame (see 56, 102 for further discussion). The number density, energy density, and pressure (n, e, p respectively) in the rest frame are then related to their computational frame counterparts by:

$$N = \gamma n \qquad 9.$$

$$\mathbf{M} = \gamma^2(\varepsilon+p)\mathbf{v} \qquad 10.$$

$$E = \gamma^2(\varepsilon+p)-p, \qquad 11.$$

where γ is the usual Lorentz factor. The numerical solution of these equations does not require a particularly large amount of CPU (central processing unit) time, but does involve a large amount of computer memory unless some simplifying geometry such as cylindrical symmetry is available. The numerical methods involve the use of a spatial mesh of fluid cells; the quantities of interest are averaged across the cell and hence the cells should be sufficiently small to insure numerical accuracy. Both space-fixed (Eulerian) and moving-boundary (Lagrangian) cells have been used. Several finite difference methods of performing the numerical integrations are in use; their accuracy and limitations are compared in (45, 114). Since the system must go out of equilibrium at some point, the calculations are truncated once a quantity such as the number density has fallen below a specified value.

Several numerical solutions of the hydrodynamic equations for heavy ion collisions have been performed (for a sample, see 7–9, 38, 111, 121, 126, 127; for other properties of nuclear fluid dynamics, see 136). Early simulations of heavy ion collisions used only a single fluid for the nuclei: the projectile and target nuclear matter became indistinguishable on impact. A way of allowing the interpenetration of the nuclei expected from a finite mean free path is to use separate fluids for each nucleus and introduce a drag term to couple them. A comparison (45) of the time evolution of the spatial density predicted by the one- and two-fluid models is shown in Figure 4. Clearly, there is less momentum transfer in the two-fluid calculations since the nuclei are partially transparent to each other.

The single-particle momentum distributions predicted by the simulations make a good test of their normalization, although such inclusive quantities are not likely to provide a detailed probe of the validity of the theoretical description. An example (45) of the comparison of the predictions with data is shown in Figure 5. The predictions of both one- and two-fluid hydrodynamics are shown for the reaction Ne+U at 250 MeV/nucleon bombarding energy. Certainly the trend of the energy spectra to steeper slopes at wider emission angles is qualitatively supported by the calculations.

2.3 *Collective Flow*

It is clear from Figure 4 that sideways collective motion or flow of the nuclear material has developed by the end of the time sequence studied. This is intuitively expected from hydrodynamics and was one of its first novel predictions. Such collective motion has been observed in heavy ion

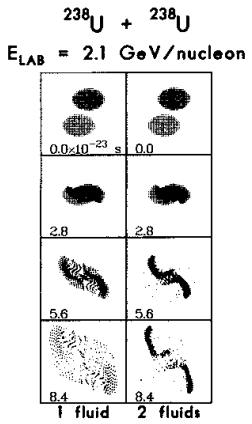

Figure 4 Matter distributions for a $^{238}U+^{238}U$ collision at a bombarding energy of 2.1 GeV/nucleon calculated with the one-fluid model (*left*) and the two-fluid model (*right*) as observed from the center-of-mass frame (45).

collisions (see 57 references therein). The magnitude of the effect is shown in Figure 6. The middle left frame shows the sideways peaking in the experimental data. Shown for comparison are the fluid dynamical predictions as well as those of two cascade models (described in the following section) in which the equation of state is neglected and only random nucleon-nucleon collisions affect the otherwise straightline motion of an individual nucleon. While the more sophisticated one-body theories, such as the Vlasov-Uehling-Uhlenbeck approach treated in the following section, also predict sideways peaked cross sections (108; see, however, 87), the measurements do indicate compressional effects in nuclear reactions. We return to another possible measure of the equation of state, meson production, in Section 3.4.

3. SIMULATIONS OF SINGLE-PARTICLE DISTRIBUTIONS

Hydrodynamics assumes that individual N-N collisions are frequent enough to maintain a local equilibrium during the course of a reaction. Although there are conditions under which this scenario may be applicable, many reactions (for example proton-induced reaction or intermediate energy, heavy ion collisions) are not subject to such simplifications. We begin our discussion of the more sophisticated methods required for these

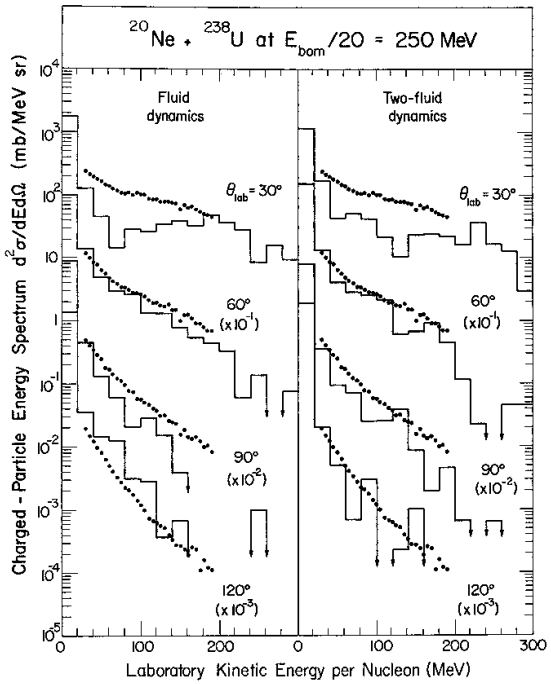

Figure 5 Charged-particle energy spectra for $^{20}Ne+^{238}U$ at a bombarding energy of 250 MeV/nucleon calculated using one-fluid (*left*) and two-fluid (*right*) hydrodynamics (45). (Data are from 68.)

reactions by examining the properties of single-particle distributions, to which many simulation techniques have been applied.

3.1 *The Intranuclear Cascade Model*

The earliest simulations of nuclear collisions used a fairly simple model (1, 17, 107): the nucleons were propagated in space by means of classical mechanics and were allowed to scatter from one another at their distance of closest approach so long as that distance was less than the classical scattering radius determined from measured cross sections. This model goes under the name of the intranuclear cascade model (we shorten the title here to "cascade model" because there have been many variants of it in the last two decades: for example 35, 36, 42, 47–51, 73, 87, 92, 124, 138).

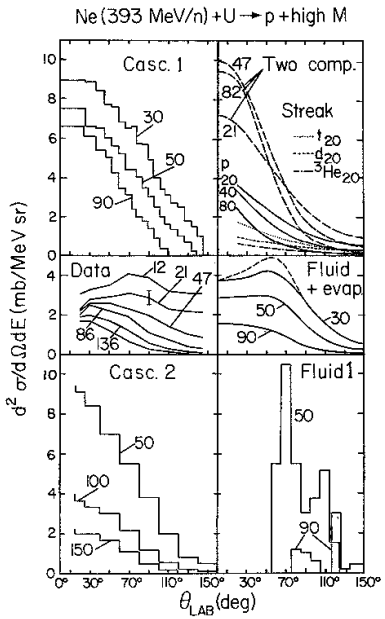

Figure 6 Comparison of data (*middle left*) with calculations for high-multiplicity-selected inclusive proton differential cross section from Ne + U at 393 MeV/nucleon. Strong forward peaking is observed in both the cascade calculations (*top* and *bottom left*) and the thermal model (*top right*). Fluid dynamical models show sideways peaking (126).

The model is computationally both fast and simple, an advantage when comparisons with experiment are required.

In the cascade model, the positions and momenta are initialized in a Monte Carlo sense, i.e. they are chosen randomly according to a prescribed distribution. For example, the momentum distribution is often chosen to be that of a zero-temperature Fermi gas, with the Fermi momentum determined by the local density. Ignored are effects arising from Pauli blocking of the N-N collisions, nuclear binding, etc, so the model cannot realistically describe fragment formation. So long as the outcome of the collision event is not sensitive to the nature of the correlations in the initialization, which are random in this model, then the model can be applied to aspects of reactions for which a classical A-body description is appropriate (see Section 4.4).

Even if one does not trust the correlations, the model is still useful. The

single-particle phase space density $f(r,p;t)$ of the classical nucleons of the cascade model should obey the Boltzmann equation with collisions but no mean field (10):

$$\frac{\partial}{\partial t}f+\mathbf{v}\cdot\frac{\partial f}{\partial \mathbf{r}}=-\int\frac{\mathrm{d}^3p_2\mathrm{d}^3p_1'\mathrm{d}^3p_2'}{(2\pi)^6}$$

$$\times v_{12}\sigma(\mathbf{p}+\mathbf{p}_2\rightarrow\mathbf{p}_1'+\mathbf{p}_2')(ff_2-f_1'f_2')\delta^3(\mathbf{p}+\mathbf{p}_2-\mathbf{p}_1'-\mathbf{p}_2'), \quad 12.$$

where v_{12} is the relative velocity of the pair of particles colliding with cross section $\sigma(\mathbf{p}+\mathbf{p}_2\rightarrow\mathbf{p}_1'+\mathbf{p}_2')$. Hence the cascade model could be regarded as a means of solving for the time evolution of $f(r,p;t)$ by taking a Monte Carlo sample and propagating it according to the microscopic physics underlying the Boltzmann equation.

Although there have been many applications of the cascade model to reactions, in particular comparisons with proton and neutron energy spectra, here we wish only to mention its use in elucidating reaction mechanisms (see 48 for a more extensive compilation of applications). The cascade model has been used to address a number of questions about the internal dynamics of a reaction, such as the approach to thermal and chemical equilibrium (49, 89). What we wish to discuss here is the time evolution of the entropy, defined in terms of the single-particle density by means of

$$S=-\frac{g}{(2\pi)^3}\int\mathrm{d}^3r\,\mathrm{d}^3p[f\ln f-(1-f)\ln(1-f)], \quad 13.$$

where g is the spin degeneracy factor. While the numerical integration over phase space can be very difficult, the two systems discussed here allow a substantial simplification.

The first example comes from heavy ion physics. Using a cascade model, Bertsch & Cugnon (19) followed the entropy produced in the central collision of two calcium nuclei at a bombarding energy of 800 MeV/nucleon in the lab. The time dependence of the calculated entropy is shown in Figure 7 (19). The entropy changes fairly rapidly during the equilibration stages of the reaction, reaching its asymptotic value not long after 10 fm/c elapsed time. The density reaches a maximum at 8 fm/c. Shown in the figure as well is the number of particles that have undergone a collision. Again, this number rises rapidly during the thermalization stage. Although the actual predicted value of the entropy may be changed by the inclusion of a nuclear binding interaction, nevertheless the simulation shows that the system expands isentropically and will pass near the critical point of the liquid-gas phase diagram. The fact that the entropy is fixed relatively early in the reaction has led to attempts at developing a

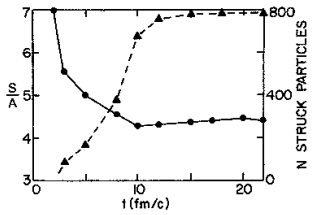

Figure 7 Time dependence of the entropy and number of nucleons that have undergone scatterings calculated for central ^{40}Ca+^{40}Ca collisions at E = 800 MeV/nucleon in a cascade model (19).

reliable method of determining the entropy from the measured products of the reactions (46).

The second example is the entropy generated in a nuclear target by the passage of a proton through it. In this calculation (26) the nuclear interaction is approximated by placing the target nucleons in a spherically symmetric step function potential. Since few nucleons are scattered out of this well during the course of the reaction, and since the momentum transferred from the projectile to the target nucleus is small, the well is spatially fixed. The reaction trajectory in excitation energy and entropy is shown in Figure 8 for those nucleons inside the target region. The system remains in a state of relatively low entropy and excitation energy throughout the reaction. Whether the system breaks up depends in part upon whether it has enough energy to carry it into the mechanical instability region (21, 34), and one can see from the figure that this occurs for the two bombarding energies shown. The simulation shows that fragmentation in intermediate energy, proton-induced reactions resembles more the breakup of cool matter near the mechanical instability region (4, 33) than it does the condensation of clusters from a hot nuclear vapor (67, 74, 81; see also 60).

3.2 *The Vlasov Equation and TDHF*

At low excitation energies, so many of the individual N-N collisions in a reaction are Pauli-blocked that the nuclear mean field plays an increasingly important role. The time-dependent Hartree-Fock (TDHF) equation represents the limit in which two-body collisions are neglected and a particle interactions only with the nuclear mean field. TDHF calculations have been successfully applied at low excitation energies to describe such phenomena as fusion and compound nucleus formation (see 55, 96, 109 for examples). The classical analogue of TDHF is the Vlasov equation, in which the time evolution of $f(r,p;t)$ is given by (10, 132)

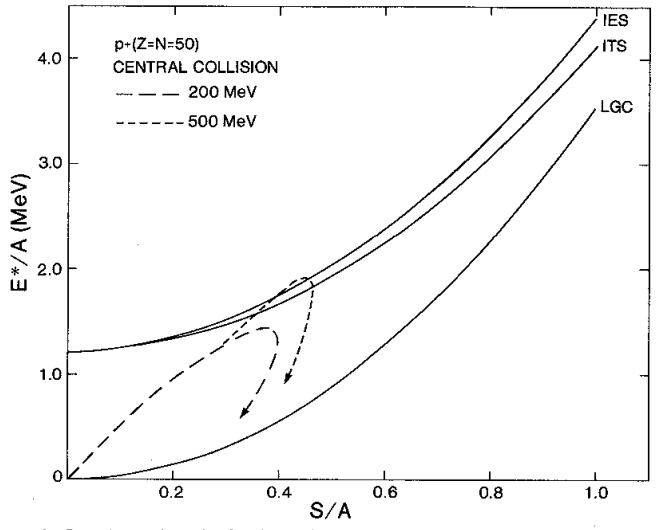

Figure 8 Reaction trajectories for the nuclear target region predicted by a cascade model for 200 and 500 MeV p+($Z = N = 50$) central collisions (*dashed lines*). Shown for comparison are the isothermal (ITS) and isentropic (IES) spinodals and the liquid-gas coexistence curve (LGC) (26).

$$\frac{\partial}{\partial t}f+\mathbf{v}\cdot\frac{\partial}{\partial \mathbf{r}}f-\nabla U\cdot\frac{\partial}{\partial \mathbf{p}}f=0. \qquad 14.$$

The predictions of the Vlasov equation should be similar to those of TDHF, and this is demonstrated in Figure 9 (3). The figure shows the density projected on the reaction plane for five different impact parameters in the $^{12}C+^{16}O$ reaction at 25 MeV/nucleon bombarding energy in the lab. The density is sampled at more than 100 fm/c after the nuclei touch. While the distributions are not identical, one can see that they are fairly similar. The Vlasov equation has also been applied with qualitative success to low energy reactions; whether it is appropriate for reactions at higher energies is addressed in the next subsection.

3.3 *A Boltzmann Equation for Fermions*

For many problems of interest in nuclear reaction studies, the simplifications made in the cascade model or the Vlasov equation are not justifiable. The Boltzmann equation for $f(r, p; t)$ includes both a mean field

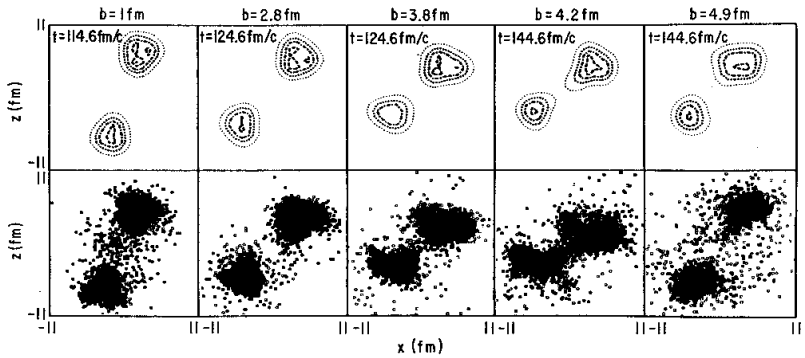

Figure 9 Density projection on the reaction plane calculated for $^{12}C+^{16}O$ collisions at $E = 25$ MeV/nucleon by means of the time-dependent Hartree-Fock (*upper part*) and Vlasov (*lower part*) equations (3).

interaction and a collision term but is not appropriate for a low temperature gas of fermions because effects such as Pauli blocking are excluded. An equation resembling the classical Boltzmann equation has been developed for fermion distributions [Nordheim (112), Landau (101), Uehling & Uhlenbeck (129); see 10, 18, 85, 116 for more detailed discussion]. Referred to as the Vlasov-Uehling-Uhlenbeck (VUU) or Landau-Vlasov equation in its application to intermediate energy, heavy ion reactions (2, 3, 5, 20, 70, 98, 99, 108, 128a; see also 119), the equation reads

$$\frac{\partial}{\partial t}f+\mathbf{v}\cdot\frac{\partial}{\partial \mathbf{r}}f-\nabla U\cdot\frac{\partial}{\partial \mathbf{p}}f=-\int\frac{d^3p_2\,d^3p_1'\,d^3p_2'}{(2\pi)^6}$$
$$\times v_{12}\sigma(\mathbf{p}+\mathbf{p}_2\rightarrow\mathbf{p}_1'+\mathbf{p}_2')[ff_2(1-f_1')(1-f_2')-f_1'f_2'(1-f)(1-f_2)]$$
$$\times\delta^3(p_1+p_2-p_1'-p_2'). \qquad 15.$$

Here the f's are the single-particle Wigner functions from which the single-particle density can be obtained via

$$\rho(\mathbf{r})=(2\pi)^{-3}\int d^3p f(\mathbf{r},\mathbf{p}). \qquad 16.$$

The effects of the Pauli principle are partly included in the collision term: the $(1-f)$ terms inhibit scattering to regions of high density in phase space. To the extent that the collisions are fast, this term may be all

that is required to avoid saturating phase space. However, there may be circumstances where the phase space density builds up faster than the collision term can deplete it, and one must find a better way to handle the consequences of Fermi-Dirac statistics. We return to this point in Sections 3.4 and 4.1.

Solutions of this equation are usually found using the Monte Carlo sampling technique. Similar problems have been solved by evaluating f and its derivatives on a spatial grid, but in general the computer memory requirements necessary to store the distribution are immense, particularly in regions of phase space where f is varying rapidly. However, progress can be made using a mesh in circumstances where the geometry can be simplified (93, 94, 115), for example in the collision of slabs of nuclear matter. In the Monte Carlo approach, f is sampled by means of test particles, N particles per nucleon, by running N events with one particle per nucleon simultaneously. The value of f, when it is needed to evaluate the Pauli blocking term for example, is calculated by summing over all N events at the same time step. The test particles are propagated by classical mechanics, with the force generated by the derivative of the nuclear mean field. Collisions are allowed to occur between test particles within each event. The simulation technique resembles closely the technique used in the cascade model, except that nuclear binding and some aspects of the Pauli principle now have been incorporated.

The extension of the Vlasov equation to include collisions changes its predictions for intermediate-energy heavy-ion reactions substantially since nuclei are largely transparent to each other in the Vlasov equation. A comparison (98) between the Vlasov and VUU predictions is shown in Figure 10. The momentum space distributions are shown after an elapsed time of 60 fm/c for a central Ar+Ca collision at a bombarding energy of 137 MeV/nucleon. In the Vlasov approach, the momentum distribution is still fairly close to that of the initial projectile and target. In contrast, the VUU approach shows far more thermalization, as is observed experimentally.

For a test of the absolute normalization of the predictions, Figure 11 shows a VUU calculation (3) of the proton spectra observed in the $^{12}C+^{16}O$ reaction at 25 MeV/nucleon. The VUU predictions have been averaged over impact parameter; the agreement is impressive. Such agreement is not always expected from the current level of sophistication of the simulations, since many codes simplify the initialization of f (e.g. uniform spherically symmetric density distributions in coordinate space) or its propagation (e.g. energy-independent N-N cross sections). Perhaps statistics plays such an important role (54, 59, 88) in the outcome of the reactions that these simplifications are irrelevant, or perhaps the effects of such simplifications

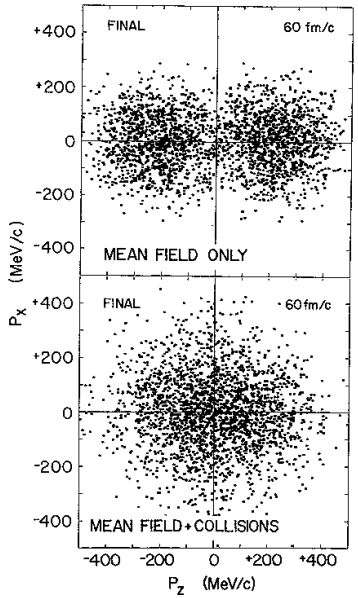

Figure 10 Final momentum-space distribution predicted for a central Ar+Ca collision at $E = 137$ MeV/nucleon by solutions of the Vlasov (*upper part*) and Vlasov-Uehling-Uhlenbeck (*lower part*) equations (98).

cancel out. In any event, the predicted normalizations for the single-particle distributions are generally within a factor of two of experiment.

3.4 *Meson Production*

So far in this review we have concentrated on the time evolution of the baryons in the nucleus. Of course, intermediate and high energy nuclear reactions can result in emission of other particles as well, such as photons, pions, and kaons. Several analytical models (see 37 and 106 for further references) have been developed to describe particle production; what we wish to mention here is the use of simulations in understanding the production mechanism and the role therein of the equation of state.

The cascade model has been used to predict photon, pion, and kaon production (for examples, see 91, 47, and 11 respectively). In this approach, meson production is envisaged to occur through the production of unstable

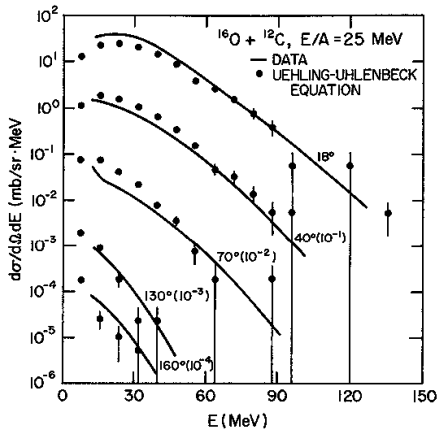

Figure 11 Proton spectra for the reaction $^{12}C+^{16}O$ at $E = 25$ MeV/nucleon. The solid line represents the data (44) while the points are the predictions of the VUU equation (3).

resonances, such as $NN \rightarrow \Delta(1230)N$, which subsequently decay. These calculations are in agreement with some of the meson production data, but not all: pion yields are typically overpredicted by a factor of two. Models that assume the establishment of thermal and chemical equilibrium also overpredict the pion yields; an example (69) is shown in Figure 12 (78). The negative pion yield per participant nucleon is shown in the figure as a function of bombarding energy for two systems: La+La (78) and Ar+KCl (77). [The term "participant nucleon" is an experimentally defined quantity that attempts to distinguish between the participant nucleons in the geometrically overlapping region of the projectile and target and the "spectator nucleons" whose momenta are not radically changed in the reaction (see 78).]

It has been suggested that the suppression of the pion yield results from nucleons losing some of their kinetic energy because of compressional effects during the early high density stages of the reaction (125). Taken at face value, Figure 12 argues that a considerable amont of energy must be removed from the system in the form of compressional potential energy before the thermal model prediction would come close to experiment. Calculations based on the VUU equation have been performed to measure the importance of the equation of state. Not all codes agree with each other on the magnitude of the effect (20, 126), but those that find a sensitivity to the equation of state tend to favor the stiff form. Currently,

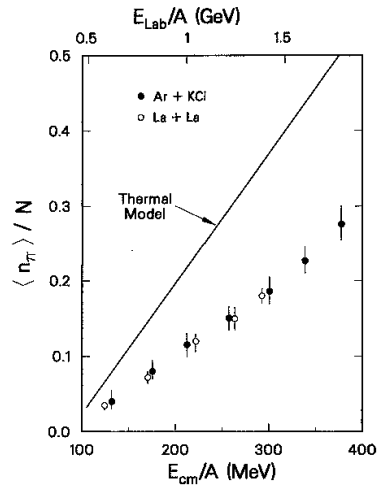

Figure 12 Ratio of the mean pion multiplicity to the number of participant nucleons as a function of incident center-of-mass energy (*bottom scale*) and laboratory energy (*top scale*). The data points are for La+La collisions (78) and Ar+KCl collisions (77). Also displayed is a thermal model prediction (based on 69) that does not include a compression term.

there remain difficulties in dealing with pion absorption and antisymmetrization effects other than those included through Pauli blocking in the collision term.

4. FLUCTUATIONS AND CORRELATIONS

The microscopic description of correlation functions and nuclear fragmentation process requires one to move beyond the one-body kinetic equations of the previous section. On the quantum mechanical level, this task is exceedingly difficult. Progress has been made by introducing fluctuations into TDHF calculations (90, 128), within which multiplicity distributions and mass spectra have been calculated for isolated nuclei evolving from given initial temperatures and densities. The calculations confirm the qualitative expectation of increasing particle multiplicities and the disappearance of large compound nuclear residues at higher temperatures. At the time of writing, these calculations have been limited to two spatial dimensions.

4.1 *Classical Equation of Motion Approach*

The development of full three-dimensional calculations began at the classical level, in which nucleon-nucleon interactions can be incorporated by means of a two-body potential. However, many of the applications to which this approach has been applied have been to single-particle distributions, particularly proton energy spectra (29–31). The difficulty in extending the calculations to fragmentation processes lies in the problem of incorporating the Pauli principle. A resolution to the problem was proposed by Wilets and coworkers (40, 134, 135; see also 56a, 62), who introduced a momentum-dependent term in the nucleon-nucleon potential between identical particles

$$V_{\text{pauli}} \propto r_{ij}^{-2} \exp\{-\alpha[(\beta \mathbf{p}_{ij} \cdot \mathbf{r}_{ij})^4 - 1]\}, \qquad 17.$$

where $\mathbf{r}_{ij}$ and $\mathbf{p}_{ij}$ are the relative positions and momenta of the two-particle pair. The parameters of the potential are adjusted to leave intact the asymptotic properties of N-N scattering. The potential is clearly repulsive in regions of high phase space density. Not only does this idea allow one to calculate A-body quantities, it also begins to address the problem of how to incorporate the Pauli principle in a way other than through N-N scattering. Even if the usual N-N scattering terms were turned off, regions of high phase space density would be avoided in this model. Unfortunately, the model has yet to be applied to fragmentation.

4.2 *Including the Pauli Principle at the Semiclassical Level*

An alternative to the use of classical equations of motion with two-body potentials is to extend the mean field methods given in Section 3. The first such calculation for nucleus-nucleus collisions was a hybrid model (63). The approach and interpenetration phase of the reaction was treated in terms of the cascade model in which binding effects were neglected. At the end of this phase, the collision term was turned off. The phase space fluctuations generated during the first stage were then propagated on an event-by-event basis by replacing each nucleon with a number of test particles whose positions and momenta were spread out with Gaussian distributions centered at the classical position and momentum of the corresponding nucleon. The resulting distribution of test particles was then propagated by solving the Vlasov equation with a density-dependent mean field such as Equation 2.

The effect of introducing the mean field is dramatic (63). Figure 13 shows the projection of the coordinate space density onto the reaction plane for a single collision of two $A = 20$ nuclei at a bombarding energy of 400 MeV/nucleon. The simulation was stopped after the main collision

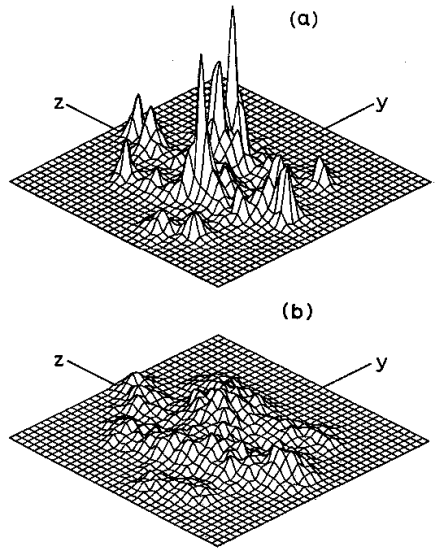

Figure 13 Contour plots of coordinate space density projected onto the reaction plane for a single collision between two $A = 20$ nuclei at a bombarding energy of 400 MeV/nucleon. The mean field interaction is included in part (*a*) and omitted in part (*b*) (63).

epoch, while the system was still expanding. The upper part of the figure shows the result of a calculation for which the mean field was included; the lower part shows the result when it was omitted. Clearly, the mean field is essential to preserve density fluctuations and produce bound clusters.

Several groups have gone further in this direction by including both a mean field and collision terms simultaneously to avoid breaking up the calculation into two distinct parts (6, 12, 14, 15, 71). Unlike the VUU calculations, these semiclassical models propagate the phase space fluctuations on an event-by-event basis. At relatively low excitation energies the fluctuations must be known with good accuracy. To ensure this accuracy, Gregoire and coworkers (71) have adopted the prescription of representing each nucleon by a number of test particles whose phase space distribution is spread out by means of Gaussian distributions. This method requires large amounts of computing time for the simulation of a single event; hence comparisons with data are not available at the time of writing. The calculations have, however, reproduced several qualitative features of nucleus-nucleus collisions at incident energies of several tens of MeV per

nucleon, such as the onset of incomplete fusion and the energy dependence of linear momentum transfer in fusion-like rections.

At higher energies, nucleon-nucleon collisions populate larger volumes of phase space, and so the numerical accuracy required for the calculation of fluctuations is reduced. One method (15), which has been used to investigate several different aspects of correlations in intermediate-energy heavy-ion collisions, uses a single test particle per nucleon, spread out in phase space with a Gaussian distribution. The savings in computation time are considerable and this allows a more thorough investigation of the reaction mechanism and comparisons with experiment. As an example, we discuss results (15) obtained for Ca+Ca collisions at a bombarding energy of 100 MeV/nucleon.

The collisions were followed for a duration of 150 fm/c, by which time most fragments had separated in coordinate space. Bound clusters were defined by linking groups of nucleons that were separated from their nearest neighbors by less than 3 fm. The momentum distributions of the reaction products predicted by the simulations showed the characteristic features expected from the participant-spectator picture: light mass systems, particularly nucleons, were widely dispersed in phase space, while heavier systems were more tightly clustered near the beam and target rapidity. The simulation allows one to check whether this observation arises mainly from geometry. To answer this question, a large number of collision events were generated, each with an impact parameter randomly chosen according to a geometrical distribution that weights peripheral collisions more heavily than central ones. At the end of each event, the fragment masses were determined. Then an average over the entire sample was made of the collision impact parameter associated with each fragment mass. This quantity is shown in Figure 14. Clearly, light fragments arise from less peripheral collisions than do heavy ones. This figure also serves as a warning against analyzing impact-parameter-averaged data with models assuming a common origin for all products.

In the simulations described, both the coulomb interaction and a phenomenological isospin-dependent mean field were included. This makes it possible to calculate isotopic distributions, such as are shown in Figure 15. The calculated distributions are peaked along the $Z = N$ curve but show a higher abundance on the neutron-rich side than the proton-rich side. This is in qualitative agreement with experiment, as are the predicted cross sections.

4.3 *Reaction Trajectories*

Numerical simulations may be particularly useful in elucidating the relation between the observed reaction products and the temporal evol-

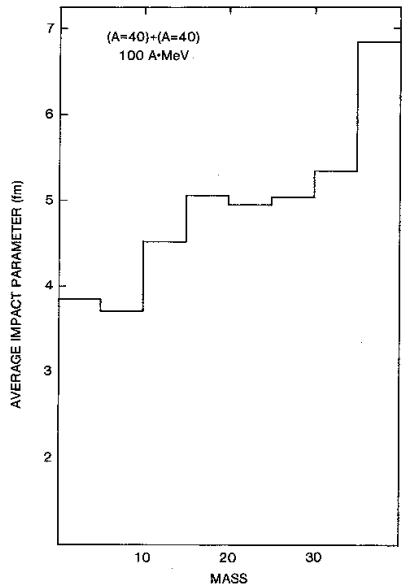

Figure 14 Average impact parameter associated with a given range of fragment mass predicted by a semiclassical calculation for Ca+Ca collisions at $E = 100$ MeV/nucleon. The bin size corresponds to 5 mass units (15).

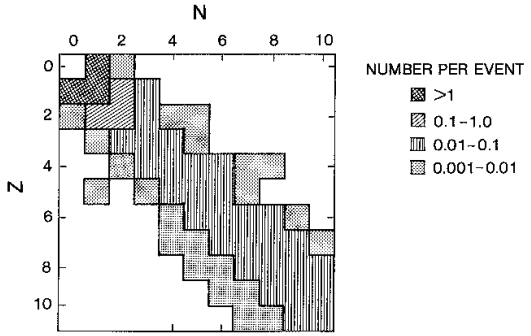

Figure 15 Isotopic yields of light fragments predicted by a semiclassical calculation for Ca+Ca collisions at $E = 100$ MeV/nucleon. The calculations were averaged over impact parameter (15).

ution of the reaction. There are several scenarios for fragment emission, each of which may have its domain of applicability. Among the possibilities are long time-scale emission such as is observed in compound systems (22, 23, 79), statistical breakup (4, 33, 54, 72, 88), and coalescence of light fragments from nucleons late in the reaction (39, 74, 75, 117).

One question of interest is whether and how the reaction is influenced by the liquid-gas coexistence region. On the atomic scale, this problem has been investigated by means of simulations for the expansion of hot argon droplets (130). The fermionic nature of their constituents makes nuclei much more difficult to handle than classical particles, so progress here has not been so rapid.

Because of the uncertainty in calculating the excitation energy of droplets in the semiclassical simulations, one method used (15) is to follow the evolution of the local coordinate and phase space densities in the vicinity of individual nucleons during a collision. At the end of the collision, it can be determined whether the nucleon has emerged as a free particle or as part of a bound cluster. The results of such an analysis for central Ca + Ca reactions at 100 MeV/nucleon bombarding energy are shown in Figures 16 and 17.

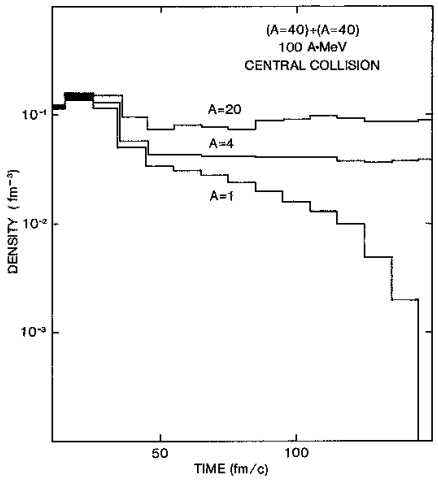

Figure 16 Temporal evolution of the average local coordinate space density in the vicinity of nucleons finally emitted as free nucleons ($A = 1$) or in bound clusters ($A = 4$, 20). The simulation is a semiclassical calculation of central Ca + Ca collisions at 100 MeV/nucleon (15).

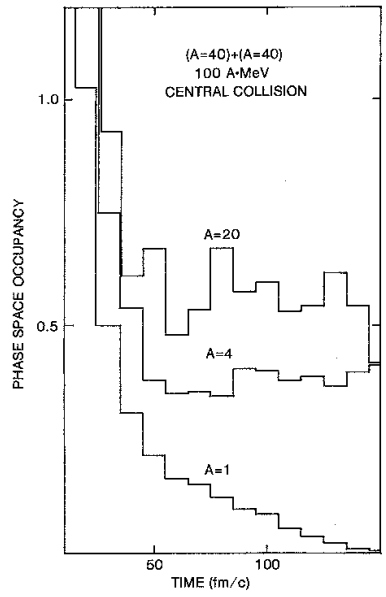

Figure 17 Temporal evolution of the average phase space density in the vicinity of nucleons finally emitted as free nucleons ($A = 1$) or in bound clusters ($A = 4$, 20). Conditions as in Figure 16 (15).

The figures show the temporal evolution of the average local coordinate space and phase space densities for free nucleons and nucleons that finally emerge in clusters of mass 4 and 20. As shown in Figure 16, after the initial phase of the reaction ($t < 30$ fm/c) the spatial density begins to decrease as the system expands. The density drops to about half of normal nuclear matter density and then the system breaks up into free nucleons and bound clusters. Although there is some oscillation in the density of the clusters, nucleons bound in clusters do not come from regions of very low density that contract into regions of higher density as the clusters are formed.

This interpretation is substantiated by the temporal evolution of the phase space densities shown in Figure 17. While the local coordinate space densities are fairly similar for all nucleons during the early violent stages of the reaction, the phase space densities are not. Particles that ultimately emerge as free nucleons are scattered into regions of low phase space density at a very early stage of the reaction. Particles that ultimately emerge

in the form of clusters remain in regions of relatively high phase space density throughout the reaction. This behavior bears qualitative resemblance to the phenomenon of percolation (13, 41; for a review, see 123).

4.4 *Two-Particle Correlation Functions*

As a final example of the application of computer simulations to nuclear reactions, we wish to examine two-particle correlation functions. The measurement of two-photon correlations at small relative momentum was advanced some time ago as a means of estimating stellar sizes (76). It was subsequently suggested that such measurements could also be used in nuclear and particle physics to measure reaction volumes (66, 95, 97, 137). Measurements of correlations between pairs of pions (61, 139), protons (140) and even nuclear fragments (43) showed the feasibility of the technique, and it has now been used extensively in nuclear physics (for a recent summary, see 65). The measured reaction volumes agree qualitatively with what is expected both intuitively and from simple numerical simulations (28, 82).

However, there are ambiguities in the measurements, and simulations may be of use in their resolution (16, 25, 82). One such observation is the variation in the measured reaction volume found as a function of the summed energy of the two particles (65). The correlations become weaker—that is, the correlation function $R(\mathbf{p}_1, \mathbf{p}_2)$ moves closer to zero—as the summed energy of the particles decreases (the relative momentum being held constant). In a simple thermal model approach to these measurements (84), the correlation function is proportional to the reciprocal of the volume, if one assumes that all particles leave the reaction region simultaneously. Thus, if the emission time scale is unimportant, the measurements can be interpreted to mean that energetic particles come from small spatial regions while slow particles come from large regions.

However, the interpretation of the energy dependence can be complicated by at least two factors, the hydrodynamic expansion of the reaction zone expected at high temperatures (113) and the long evaporative time scale expected at low temperatures. A cascade model simulation has been used to assess the importance of the finite emission time effect (25). The two-proton correlation function was simulated for emission from a single nucleus at finite temperature. Nuclear binding was included by putting the nucleons in a fixed step function potential well, as was described in the entropy calculation used to generate Figure 8. The correlation function obtained from the analysis of 20,000 events is shown in Figure 18. Three energy cuts have been made in generating the computer "data" for the correlation function shown in the figure.

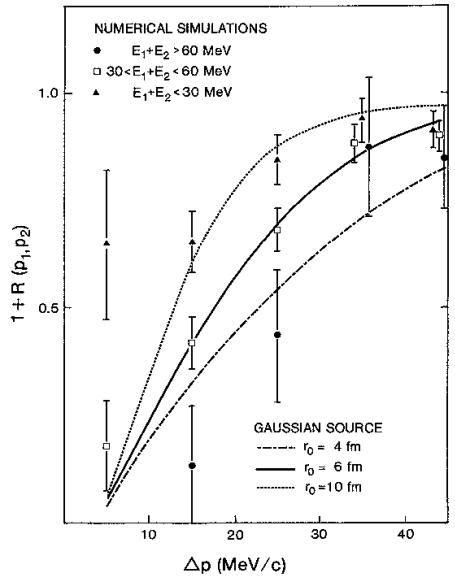

Figure 18 A cascade model simulation of two-proton correlation functions predicted for an isolated nucleus of fixed size at an initial temperature of 15 MeV. The smooth curves correspond to predictions for Gaussian sources of zero lifetime and radius parameters of $r_0 = 4$, 6, and 10 fm (25).

The smooth curves in the figure are the results from an analytical calculation of the correlation function assuming zero-lifetime source of Gaussian spatial extent (95). The Gaussian is characterized by a parameter r_0, which has the values 4, 6, and 10 fm in the figure. The apparent change in the size of the source region predicted by the simulation as obtained from the analysis is very similar to what is observed experimentally. However, in the simulation the spatial dimension of the source is fixed. The simulations show that the variation in apparent size arises from the longer emission times associated with the lower energy ejectiles.

5. SUMMARY AND OUTLOOK

The speed and storage capabilities of modern computers have allowed nuclear reaction studies to move beyond specific reactions that lend them-

selves to analytical treatment and toward an accurate description of the complex reactions found in heavy ion physics. The success achieved in describing reactions at the low (TDHF, Vlasov equation) and high (cascade) extremes of bombarding energy have encourged the development of more sophisticated simulations that include the nuclear mean field, individual N-N collisions, and antisymmetrization effects. These calculations have been successful at the quantitative level in comparison with single-particle inclusive measurements. The incorporation of fluctuations in the simulations at the semiclassical level has opened up the study of fragment formation and two-particle correlation functions. Because of the large CPU-time requirements of such simulations, only qualitative comparisons with data are currently warranted.

The simulations allow the investigation of such questions as the nature of the nuclear equation of state at high densities and the effects of the nuclear liquid-gas phase transition on fragmentation processes. Evidence is present within the simulations for phase transition effects, although the extraction of an experimental signature of the effects remains elusive. At high densities, the equation of state may be making itself felt through collective flow and reduced meson production. The inclusion of antisymmetrization effects through more than the Uehling-Uhlenbeck collision term will allow one to probe more deeply into the high density phase of energetic reactions.

At very high energy densities, one expects (105) that the parton constituents of the nucleons will become deconfined and form a plasma state. Simulations based on parton degrees of freedom have already been used to estimate the conditions achievable in ultrarelativistic heavy ion collisions (24) and undoubtedly will play an important role in the search for experimental signatures of this state. Progress in the development of a tractable transport theory is expected to be rapid in the coming years (64, 58, 80).

As is always the case with computer-based research, progress is at least in part subject to machine limitations. However, the near-term future of this field of study looks bright for at least two reasons: the easy accessibility of supercomputers to an increasing number of researchers and the availability of modestly priced, yet powerful smaller scale processors that lend themselves to dedicated use for simulation purposes. Further, the application of computer animation techniques as exemplified by Figure 1 will allow us to see inside a collision in a manner never before available.

ACKNOWLEDGMENT

The author wishes to thank the Natural Sciences and Engineering Research Council of Canada for financial support.

Literature Cited

1. Abate, E., Bellini, G., Fiorini, E., Ratti, S. *Nuovo Cimento* 22: 1206 (1961)
2. Aichelin, J. *Phys. Lett.* 164B: 261–64 (1985)
3. Aichelin, J., Bertsch, G. *Phys. Rev.* C31: 1730–38 (1985)
4. Aichelin, J., Hufner, J., Ibarra, R. *Phys. Rev.* C30: 107–18 (1984)
5. Aichelin, J., Stocker, H. *Phys. Lett.* 163B: 59–65 (1985)
6. Aichelin, J., Stocker, H. *Phys. Lett.* 176: 14 (1986)
7. Amsden, A. A., Bertsch, G. F., Harlow, F. H., Nix, J. R. *Phys. Rev. Lett.* 35: 905–8 (1975)
8. Amsden, A. A., Ginocchio, J. N., Harlow, F. H., Nix, J. R., Danos, M., et al. *Phys. Rev. Lett.* 38: 1055–58 (1977)
9. Amsden, A. A., Harlow, F. H., Nix, J. R. *Phys. Rev.* C15: 2059–71 (1977)
10. Balescu, R. *Equilibrium and Nonequilibrium Statistical Mechanics.* New York: Wiley (1975)
11. Barz, H. W., Iwe, H. *Phys. Lett.* 143B: 55–59 (1984)
12. Bauer, W., Bertsch, G. F., Das Gupta, S. *Mich. State Univ. Rep.* (1986)
13. Bauer, W., Dean, D. R., Mosel, U., Post, U. *Phys. Lett.* 150B: 53–56 (1985)
14. Beauvais, G. E., Boal, D. H., Glosli, J. *Nucl. Phys. A.* In press (1987)
15. Beauvais, G. E., Boal, D. H., Wong, J. C. K. *Phys. Rev.* C35: 545–55 (1987)
16. Bernstein, M. A., Friedman, W. A., Lynch, W. G. *Phys. Rev.* C29: 132–38; C30: 412 (E) (1984)
17. Bertini, H. W. *Phys. Rev.* 131: 1801–21 (1963); 138: AB2 (E) (1965)
18. Bertsch, G. *Prog. Part. Nucl. Phys.* 4: 483 (1980)
19. Bertsch, G., Cugnon, J. *Phys. Rev.* C24: 2514–20 (1981)
20. Bertsch, G., Kruse, H., Das Gupta, S. *Phys. Rev.* C29: 673–75 (1984)
21. Bertsch, G., Siemens, P. J. *Phys. Lett.* 126B: 9–12 (1983)
22. Blann, M. *Ann. Rev. Nucl. Sci.* 25: 123–66 (1975)
23. Blatt, J. M., Weisskopf, V. F. *Theoretical Nuclear Physics.* New York: Wiley (1952)
24. Boal, D. H. *Phys. Rev.* C33: 2206–8 (1986)
25. Boal, D. H., DeGuise, H. *Phys. Rev. Lett.* 57: 2901–4 (1986)
26. Boal, D. H., Goodman, A. L. *Phys. Rev.* C33: 1690–98 (1986)
27. Boal, D. H., Reid, J. H. *Phys. Rev.* C29: 973–84 (1984)
28. Boal, D. H., Shillcock, J. C. *Phys. Rev.* C33: 549–56 (1986)
29. Bodmer, A. R., Panos, C. N. *Phys. Rev.* C15: 1342–58 (1977)
30. Bodmer, A. R., Panos, C. N. *Nucl. Phys.* A356: 517–22 (1981)
31. Bodmer, A. R., Panos, C. N., Mackellar, A. D. *Phys. Rev.* C22: 1025–54 (1980)
32. Bonche, P., Levit, S., Vautherin, D. *Nucl. Phys.* A436: 265–93 (1985)
33. Bondorf, J. *Nucl. Phys.* A387: 25c–36c (1982)
34. Bondorf, J. P., Donangelo, R., Shulz, H., Sneppen, K. *Phys. Lett.* 162B: 30–34 (1985)
35. Bondorf, J. P., Feldmeier, H. T., Garpman, S., Halbert, E. C. *Phys. Lett.* 65B: 217–20 (1976)
36. Bondorf, J. P., Siemens, P. J., Garpman, S., Halbert, E. *Z. Phys.* 279: 385–94 (1976)
37. Braun-Munzinger, P., Stachel, J. *Ann. Rev. Nucl. Part. Sci.* 37: 97 (1987)
38. Buchwald, G., Graebner, G., Theis, J., Maruhn, J. A., Greiner, W., Stocker, H. *Phys. Rev.* C28: 1119–22 (1983)
39. Butler, S. T., Pearson, C. A. *Phys. Rev. Lett.* 7: 69–71 (1961)
40. Callaway, D. J. E., Wilets, L., Yariv, Y. *Nucl. Phys.* A327: 250–68 (1979)
41. Campi, X., Desbois, J., Lipparini, E. *Phys. Lett.* 142B: 8–13 (1984)
42. Chen, K., Fraenkel, Z., Friedlander, G., Grover, J. R., Miller, J. M., Shimamoto, Y. *Phys. Rev.* 166: 949–67 (1968)
43. Chitwood, C. B., Aichelin, J., Boal, D. H., Bertsch, G., Fields, D. J., et al. *Phys. Rev. Lett.* 54: 302–5 (1985)
44. Chitwood, C. B., Fields, D. J., Gelbke, C. K., Klesch, D. R., Lynch, W. G., et al. *Phys. Rev.* C34: 858–71 (1986)
45. Clare, R. B., Strottman, D. *Phys. Rep.* 141: 177–280 (1985)
46. Csernai, L. P., Kapusta, J. *Phys. Rep.* 131: 223–318 (1986)
47. Cugnon, J. *Phys. Rev.* C22: 1885–96 (1980)
48. Cugnon, J. Lectures given at the Cargese Summer School (1984)
49. Cugnon, J., Jaminon, M. *Phys. Lett.* 123B: 155–59 (1983)
50. Cugnon, J., Knoll, J., Randrup, J. *Nucl. Phys.* A360: 444–58 (1981)
51. Cugnon, J., Mizutani, T., Vandermeulen, J. *Nucl. Phys.* A352: 505–34 (1981)
52. Curtin, M. W., Toki, H., Scott, D. K. *Phys. Lett.* 123B: 289–92 (1983)
53. Danielewicz, P. *Nucl. Phys.* A314: 465–84 (1979)

54. Das Gupta, S., Mekjian, A. Z. *Phys. Rep.* 72: 131–83 (1981)
55. Davies, K. T. R., Devi, K. R. S., Koonin, S. E., Strayer, M. R. In *Heavy Ion Science*, ed. D. A. Bromley. New York: Plenum (1984)
56. de Groot, S. R., van Leeuwen, W. A., van Weert, Ch. G. *Relativistic Kinetic Theory*. Amsterdam: North Holland (1980)
56a. Dorso, C., Duarte, S., Randrup, J. *Phys. Lett. B*. In press (1987)
57. Doss, K. G. R., Gustafsson, H. A., Gutbrod, H. H., Kampert, K. H., Kolb, B., et al. *Phys. Rev. Lett.* 57: 302–5 (1986)
58. Elze, H.-Th., Gyulassy, M., Vasak, D. *Lawrence Berkeley Lab. Rep. 21137* (1986)
59. Fai, G., Randrup, J. *Nucl. Phys.* A381: 557–76 (1982)
60. Fischer, M. E. *Physics* 3: 255 (1967)
61. Fung, S. Y., Gorn, W., Kiernan, G. P., Lu, J. J., Oh, Y. T., Poe, R. T. *Phys. Rev. Lett.* 41: 1592–94 (1978)
62. Gale, C., Bertsch, G., Das Gupta, S. *Univ. Minn. Rep.* (1986)
63. Gale, C., Das Gupta, S. *Phys. Lett.* 162B: 35–38 (1985)
64. Gavin, S. *Nucl. Phys.* A435: 826–43 (1985)
65. Gelbke, C. K., Boal, D. H. *Prog. Nucl. Part. Phys.* In press (1987)
66. Goldhaber, G., Goldhaber, S., Lee, W., Pais, A. *Phys. Rev.* 20: 300–12 (1960)
67. Goodman, A. L., Kapusta, J. I., Mekjian, A., *Phys. Rev.* C30: 851–65 (1984)
68. Gosset, J., Gutbrod, H. H., Meyer, W. G., Poskanzer, A. M., Sandoval, A., et al. *Phys. Rev.* C16: 629–57 (1977)
69. Gosset, J., Kapusta, J. I., Westfall, G. D. *Phys. Rev.* C18: 844–55 (1978)
70. Gregoire, C., Remaud, B., Scheuter, F., Sebille, F. *Nucl. Phys.* A436: 365–96 (1985)
71. Gregoire, C., Remaud, B., Sebille, F., Vinet, L., Raffray, Y. GANIL preprint (1986)
72. Gross, D. H. E., Satpathy, L., Meng, T.-C., Satpathy, M. *Z. Phys.* A309: 41–48 (1982)
73. Gudima, K. K., Toneev, V. D. *Sov. J. Nucl. Phys.* 27: 351 (1978)
74. Gutbrod, H. H., Sandoval, A., Johansen, P. J., Poskanzer, A. M., Gosset, J., et al. *Phys. Rev. Lett.* 37: 667–70 (1976)
75. Gyulassy, M., Frankel, K., Remler, E. A. *Nucl. Phys.* A402: 596–611 (1983)
76. Hanbury-Brown, R., Twiss, R. Q. *Nature* 178: 1046 (1956)
77. Harris, J. W., Bock, R., Brockman, R., Sandoval, A., Stock, R., et al. *Phys. Lett.* 153B: 377–81 (1985)
78. Harris, J. W., Odyniec, G., Pugh, H. G., Schroeder, L. S., Tinckhell, M. L., et al. *Lawrence Berkeley Lab. Rep. LBL-22003* (1986)
79. Hauser, W., Feshbach, H. *Phys. Rev.* 87: 366–73 (1952)
80. Heinz, U. *Phys. Rev. Lett.* 51: 351–54 (1983)
81. Hirsch, A. S., Bujak, A., Finn, J. E., Gutay, L. J., Minich, R. W., et al. *Phys. Rev.* C29: 508–25 (1984)
82. Humanic, T. J. *Phys. Rev.* C34: 191–95 (1986)
82a. Jacak, B. V., Westfall, G. D., Gelbke, C. K., Harwood, L. H., Lynch, W. G., et al. *Phys. Rev. Lett.* 51: 1846–49 (1983)
83. Jaqaman, H. R., Mekjian, A. Z., Zamick, L. *Phys. Rev.* C27: 2782–91 (1983)
84. Jennings, B. K., Boal, D. H., Shillcock, J. C. *Phys. Rev.* C33: 1303–6 (1986)
85. Kadanoff, L. P., Baym, G. *Quantum Statistical Mechanics*. New York: Benjamin (1962)
86. Kikuchi, K., Kawai, M. *Nuclear Reactions at High Energy*. Amsterdam: North Holland (1968)
87. Kitazoe, Y., Sano, M., Yamamura, Y., Furutani, H., Yamamoto, K. *Phys. Rev.* C29: 828–36 (1984)
88. Knoll, J. *Phys. Rev.* C20: 773–80 (1979)
89. Knoll, J., Randrup, J. *Nucl. Phys.* A324: 445–63 (1979)
90. Knoll, J., Strack, B. *Phys. Lett.* 149B: 45–49 (1984)
91. Ko, C. M., Bertsch, G., Aichelin, J. *Phys. Rev.* C31: 2324–26 (1985)
92. Kodama, T., Duarte, S. B., Chung, K. C., Nazareth, R. A. M. S. *Phys. Rev. Lett.* 49: 536–39 (1982)
93. Kohler, H. S. *Nucl. Phys.* A378: 159–80 (1982)
94. Kohler, H. S., Neilsson, B. S. *Nucl. Phys.* A417: 541–63 (1984)
95. Koonin, S. E. *Phys. Lett.* 70B: 43–47 (1977)
96. Koonin, S. E., Davies, K. T. R., Maruhn-Rezwani, V., Feldmeier, H., Kreiger, S. J., Negele, J. W. *Phys. Rev.* C15: 1359–74 (1977)
97. Kopylov, G. I. *Phys. Lett.* 50B: 472–74 (1974)
98. Kruse, H., Jacak, B. V., Molitoris, J. J., Westfall, G. D., Stocker, H. *Phys. Rev.* C31: 1770–74 (1985)
99. Kruse, H., Jacak, B. V., Stocker, H. *Phys. Rev. Lett.* 54: 289–92 (1985)
100. Lamb, D. Q., Lattimer, J. M., Pethick, C. J., Ravenhall, D. G. *Phys. Rev. Lett.* 41: 1623–26 (1978)

101. Landau, L. D., *Phys. Z. Sov. Union* 10: 154 (1936)
102. Landau, L. D., Lifshitz, E. M. *Fluid Mechanics*. Oxford: Pergamon (1959)
103. Lattimer, J. M., Pethick, C. J., Ravenhall, D. G., Lamb, D. Q. *Nucl. Phys.* A432: 646–742 (1985)
104. Lopez, J. A., Siemens, P. J. *Nucl. Phys.* A431: 728–44 (1984)
105. Kajantie, K., McLerran, L. *Ann. Rev. Nucl. Part. Sci.* 37: 293 (1987)
106. Mekjian, A. Z. *Nucl. Phys.* A384: 492–536 (1982)
107. Metropolis, N., Bivins, R., Storm, M., Miller, J. M., Friedlander, G., Turkevich, A. *Phys. Rev.* 110: 185–203 (1958)
108. Molitoris, J. J., Stocker, H. *Phys. Lett.* 162B: 47–54 (1985)
109. Negele, J. *Rev. Mod. Phys.* 54: 913–1015 (1982)
110. Nix, J. R. *Prog. Part. Nucl. Phys.* 2: 237–84 (1979)
111. Nix, J. R., Strottman, D., Yariv, Y., Fraenkel, Z. *Phys. Rev.* C25: 2491–97 (1982)
112. Nordheim, L. W. *Proc. R. Soc. Ser. A* 119: 689 (1928)
113. Pratt, S. *Phys. Rev. Lett.* 53: 1219–21 (1984)
114. Potter, D. *Computational Physics*. New York: Wiley (1973)
115. Randrup, J. *Nucl. Phys.* A314: 429–53 (1979)
116. Remler, E. A. *Ann. Phys.* 95: 455–95 (1975)
117. Remler, E. A. *Ann. Phys.* 136: 293–316 (1981)
118. Sauer, G., Chandra, H., Mosel, U. *Nucl. Phys.* A264: 221–43 (1976)
119. Sebille, F., Remaud, B. *Nucl. Phys.* A420: 141–61 (1984)
120. Shulz, H., Munchow, L., Ropke, G., Schmidt, M. *Phys. Lett.* 119B: 2–16 (1982)
121. Sierk, A. J., Nix, J. R. *Phys. Rev.* C22: 1920–26 (1980)
122. Deleted in proof
123. Stauffer, D. *Phys. Rep.* 54: 1–74 (1979)
124. Stevenson, J. D. *Phys. Rev. Lett.* 41: 1702–5 (1978)
125. Stock, R. *Phys. Rep.* 135: 259–315 (1986)
126. Stocker, H., Greiner, W. *Phys. Rep.* 137: 277–392 (1986)
127. Stocker, H., Maruhn, J. A., Greiner, W. *Phys. Rev. Lett.* 44: 725–28 (1980)
128. Strack, B., Knoll, J. *Z. Phys.* A315: 249–50 (1984)
128a. Tsang, M. B., Ronningen, R. M., Bertsch, G., Chen, Z., Chitwood, C. B., et al. *Phys. Rev. Lett.* 57: 559–62 (1986)
129. Uehling, E. A., Uhlenbeck, G. E. *Phys. Rev.* 43: 552 (1933)
130. Vincentini, A., Jacucci, G., Pandharipande, V. R. *Phys. Rev.* C31: 1783–93 (1985)
131. Vinet, L., Sebille, F., Gregoire, C., Remaud, B., Shuck, P. *Phys. Lett.* 172B: 17–22 (1986)
132. Vlasov, A. *Zh. Eksp. Teor. Fiz.* 8: 291 (1938)
133. Weiner, R., Weststrom, M. *Nucl. Phys.* A286: 282–96 (1977)
134. Wilets, L., Henley, E. M., Kraft, M., Mackellar, A. D. *Nucl. Phys.* A282: 341 (1977)
135. Wilets, L., Yariv, Y., Chestnut, R. *Nucl. Phys.* A301: 359–64 (1978)
136. Wong, C. Y., Welton, T. A., Maruhn, J. A. *Phys. Rev.* C15: 1558–70 (1977)
137. Yano, F. B., Koonin, S. E. *Phys. Lett.* 78B: 556–59 (1978)
138. Yariv, Y., Fraenkel, Z. *Phys. Rev.* C20: 2227–43 (1979)
139. Zajc, W. A., Bistirlich, J. A., Bossingham, R. J., Bowman, H. R., Clawson, C. W., et al. *Phys. Rev.* C29: 2173–87 (1984)
140. Zarbakhsh, F., Sagle, A. L., Brochard, F., Mulera, T. A., Perrez-Mendez, V., et al. *Phys. Rev. Lett.* 46: 1268–70 (1981)